Sustainable Materials and Technologies 42 (2024) e01177

Contents lists available at ScienceDirect

Sustainable Materials and Technologies

journal homepage: www.elsevier.com/locate/susmat

Enhancing CO_2 capture performance through activation of olive pomace biochar: A comparative study of physical and chemical methods

A. Alcazar-Ruiz [a,1], S. Maisano [b,*,1,1], V. Chiodo [b], F. Urbani [b], F. Dorado [a], L. Sanchez-Silva [a,*]

[a] Department of Chemical Engineering, University of Castilla –La Mancha, Avda. Camilo José Cela 12, 13071 Ciudad Real, Spain
[b] CNR - ITAE, Institute for Advanced Energy Technologies "Nicola Giordano", Via S. Lucia Sopra Contesse 5, 98126 Messina, Italy

ARTICLE INFO

Keywords:
Olive pomace
Sustainable adsorbents
KOH activation
CO_2 activation
CO_2 storage

ABSTRACT

This work contributes understanding technical feasibility use of an agro-industrial waste as raw material for CO_2 capture. Physical and chemical activation treatments to enhance adsorption properties of exhausts olive pomace biochar were investigated. Innovatively, the effects of different kinds of activating agents (steam, CO_2, H_3PO_4 and KOH) on activated biocarbon's properties were deeply examined, also through an original high-pressure thermobalance, that is enabled higher initial sample weights, temperatures, and pressures compared to those employed in conventional methods.

The activation conditions significantly affect the biochar morphology and CO_2 adsorption capacity. Chemical activation, particularly with KOH, produced highly microporous structures, greatly enhancing CO_2 adsorption. Specifically, KOH activation achieved adsorption capacities of up to 3.04 mmol/g at 30 °C and 10 bar. Textural analysis showed that KOH activation primarily increased microporosity, while other methods produced both micropores and mesopores. Interestingly, acid and physical activations were less effective, as they reduced CO_2 adsorption due to changes in the internal structure. Thus, olive pomace proves to be a promising precursor for developing efficient biochar adsorbents. The use of KOH as an activating agent particularly stands out, achieving notable CO_2 adsorption capacities.

1. Introduction

Nowadays, CO_2 emissions are the main responsible cause for global climate change. Comparing to preindustrial period, the concentration of CO_2 in the air has increased by more than 54.4 % [1].Therefore, developing technologies to restrain CO_2 emissions and reduce atmospheric CO_2 concentrations to achieve carbon neutrality results essential.

Liquid adsorbents, such as liquid amines and aqueous alkalis, find extensive use in various industries. However, the volatile loss and corrosion to the instrument are the major problems of liquid adsorbents [2]. Thus, to delve into the enhanced viability of CO_2 adsorbents, researchers have turned to solid materials for carbon capture applications [3]. Solid adsorbents, including metal−organic frameworks (MOFs) [4], zeolites [5], and carbonaceous materials [6], show promise due to their high CO_2 capacity, ease of modification, cost-effectiveness, and overall stability. From the latter, biochar emerges as a noteworthy candidate. It is a carbonaceous material typically produced through biomass pyrolysis in an inert atmosphere. Biomass from agricultural waste as the precursor of biochar has a considerable production globally, promoting biochar production in large quantities. Moreover, a notable advantage of these materials is that they sequester atmospheric carbon during their growth, consequently mitigating the carbon footprint of the end product [7]. Another important benefit of activated biochars derived from biomass sources are their high availability and low cost of production [8]. In some cases, these wastes could provide a solution according to the circular economy of certain agro-industries.

The olive oil sector plays an important role on mediterranean agro-industries from an economical point of view. Spain is also among the major producer and exporter of olive oil in Europe [7]. There are several reasons why olive pomace is a good candidate as a sustainable raw material to produce biochars. It is the main subproduct obtained from olive oil extraction procedure [9]. However, it has a high amount of fixed and elemental carbon content. In addition, its low ash content means it efficient for producing microporous activated carbons [10,11].

Compared with other typical solid CO_2 adsorbents, biochar mainly

* Corresponding authors.
E-mail addresses: susanna.maisano@itae.cnr.it (S. Maisano), marialuz.sanchez@uclm.es (L. Sanchez-Silva).
[1] Both authors can be considered as 1st author with equal contribution

https://doi.org/10.1016/j.susmat.2024.e01177
Received 6 June 2024; Received in revised form 8 October 2024; Accepted 10 November 2024
Available online 14 November 2024

relies on physical properties to achieve adsorption, transportation and storage of CO_2. The porosity of biochar is a crucial factor for effective CO_2 capture. Consequently, the activation of biochar becomes an essential step in enhancing its porous structure. The main biochar activation methods are physical and chemical activation. The former consists in partial gasification in a CO_2 or steam atmosphere among other gasses [7]. It reacts with biochar under high temperature conditions and removing the volatile to generate abundant porosity [2,12,13]. Physical activation is a relatively eco-friendly and cost-effective approach for increasing textural properties [14]. Although physical biochar activation is more moderate and less polluting, its activation strength is lower than that of the chemical activation method [2]. Rashidi et al. studied CO_2 activated biochars made from palm kernel shells at 850 °C for 1 h. These materials demonstrate a capacity CO_2 adsorption rate of 2.13 mmol/g along with excellent regeneration performance of stability after many cycles [15]. Puig-Gamero et al. used olive stone as a precursor to synthesize activated biochar using two agents (steam and CO_2). The optimization of temperature, pressure, flow rate, and holding time was conducted to maximize the CO_2 adsorption capacity of the resulting biochar. For H_2O activation, the established activation conditions were 900 °C while CO_2 activation was set at 1000 °C for 30 min and 1 bar [7]. Furthermore, the activated biochars demonstrated respectable CO_2 adsorption capacity of 4.28 and 4.66 mmol/g at 30 °C and 10 bar, with BET specific surface area of 955.06 and 1190.65 m2/g, and total pore volumes of 0.44 and 0.69 cm^3/g for CO_2 and H_2O activation, respectively. Moreover, air activation has the capability to generate activated carbon featuring diverse pore sizes and surface areas. However, its application is less common due to the potential risks associated with the oxidation and combustion of the precursor material [16].

In contrast, chemical activation of biochar relies on the reaction between active chemical compounds, either acids (e.g., H_3PO_4, HNO_3, and H_2O_2), alkaline (e.g., KOH and NaOH), or salts (e.g., K_2CO_3, $ZnCl_2$, and $MgCl_2$), and carbon to achieve the purpose of porous structure formation [2,17,18]. Porosity is directly influenced by the volume of the chemical agent used and the activation temperature [14]. However, precise control of chemical activation conditions is imperative to prevent the destruction and structural collapse of biochar, given the high reactivity of activation agents. Acevedo et al. investigated the preparation of porous activated carbon from the chemical activation of African palm shells. They utilized solutions of $Fe(NO_3)_3$ and $Cu(NO_3)_2$ with varying concentrations and conducted the activation process at two different temperatures of 700 °C and 800 °C. These results indicated that the activation process had notable effects on the textural parameters, elemental composition, and proximal composition of the obtained solids. Additionally, the CO_2 uptake values at low pressures were between from 1.82 to 5.68 mmol/g [19]. Cao et al. recommended the use of chemical activation instead of physical activation using the steam method because it consumes less energy. Among the various activators, they suggested the use of KOH due to its less harmful environmental impact compared to $ZnCl_2$ or H_3PO_4 [20]. KOH activation is one of the most common and best ways to produce well-developed porous biochar. Li et al. synthesized activated biochar using KOH activation from water chestnut shells, achieving a surface area of 3.401 m^2/g and a total pore volume of 2.50 cm^3/g [21]. Nevertheless, there are still challenges for biochar-based carbon capture. The production procedure is closely dependent on the porous structure of biochar. During the activation process, the surface properties of activated biochars are influenced by several parameters of which precursor type, and activation agent, activation temperature are being the most dominant ones [12,22,23].

Although production of CO_2 sorbents from residual materials is widely reported in literature, few research works have investigated on effect of the different activation treatments on olive pomace activated biocarbon's properties. Hence, this work aims to highlight the influence both physical and chemical activation methods on olive pomace derived biochar. Thus, different activation agents, such as, steam and CO_2 (physical activation) in parallel with H_3PO_4 and KOH at different concentrations (chemical activation), were used to produce activated biocarbons to apply as adsorbents in CO_2 separation.

The novelty of the paper can be identified mainly on two aspects: the first one is the deeply analysis of the activation methodologies (both physical and chemical) and conversion conditions that influence the properties of activated biocarbon derived from exhausts olive pomace, identifying promising ways for providing control of the adsorbent pore diameter and structure, while the second one is the evaluation of activated biocarbon performances into CO_2 separation through an original high-pressure thermobalance enables to higher initial sample weights, temperatures, and pressures compared to those employed in conventional methods.

2. Materials and methodology

2.1. Biomass feed

Olive pomace (OP) valorized in this work was provided from Aceites García de la Cruz olive oil mill from Madridejos (Toledo, Spain). This OP comes from 2021/2022 olive harvest of the cornicabra variety. The biomass was oven-dried for 24 h at 100 °C, and then ground and sieved to obtain an average particle size ranging less than 0.2 mm.

2.2. Activated biochar preparation

In this study, two different methodologies of activated carbon production were carried out, as illustrated in Fig. 1.

Specifically, both chemical and physical activation methods were considered. The pyrolysis and activation processes were conducted at a facility located at CNR-ITAE in Messina. The carbonization was performed in an electrically heated furnace with a fixed-bed reactor made of a stainless-steel tube. The details of the plant can be found in previous articles by the authors [24,25].

For chemical activation, two methods were employed: one acidic and the other basic. The acidic activation used 85 % phosphoric acid (H_3PO_4) in two ratios relative to the biomass (1:1 and 1:3) [26,27]. In the initial phase, about 20 g of olive pomace (OP) were pyrolyzed in a fixed-bed reactor at 600 °C, with a heating rate of 10 °C/min and an argon flow of 150 ml/min. This sample was labeled OP-C (as the reference carbonized OP sample). Afterward, the biochar obtained was stirred at 85 °C with 300 ml of the H_3PO_4 solution in distilled water, using the appropriate ratio for each test. The mixture was kept at this temperature for 6 h to allow the acid to fully penetrate the biochar structure. The solid product was then filtered from the solution and dried in an oven at 110 °C for 12 h to ensure the removal of moisture. The final carbonization and activation steps of the produced biochar were conducted at 650 °C, with a heating rate of 7 °C/min and an argon flow of 160 ml/min for 1 h.

The resulting charcoal was washed with hot distilled water until reaching a neutral pH of around 6–7 and then dried again at 110 °C for 12 h. The basic activation process, on the other hand, was carried out using KOH in ratios of 1:2 and 1:4 with the biomass. The detailed experimental procedure has been described in previous work by the authors [24]. In brief, 20 g of biomass were initially pyrolyzed at 600 °C and then impregnated with a KOH solution in the specified ratios. The char/KOH mixture was then evaporated at 80 °C, followed by activation at 800 °C for 1 h in an argon atmosphere. The resulting activated charcoal was washed and neutralized to a pH of 7 using a 1 M HCl solution, and subsequently dried at 60 °C for 12 h [28,29]. The samples produced through chemical activation were labeled OP-1:1H_3PO_4, OP-1:3H_3PO_4, OP-1:2KOH, and OP-1:4KOH.

In this research, a single-step physical activation with steam and carbon dioxide was carried out in a High Pressure Thermobalance (Linseis STA HP/2 HP-TGA DSC). The schematic and detailed description of the experimental system can be found elsewhere [30,31]. Firstly, OP was heated from room temperature to 600 °C at a heating rate of

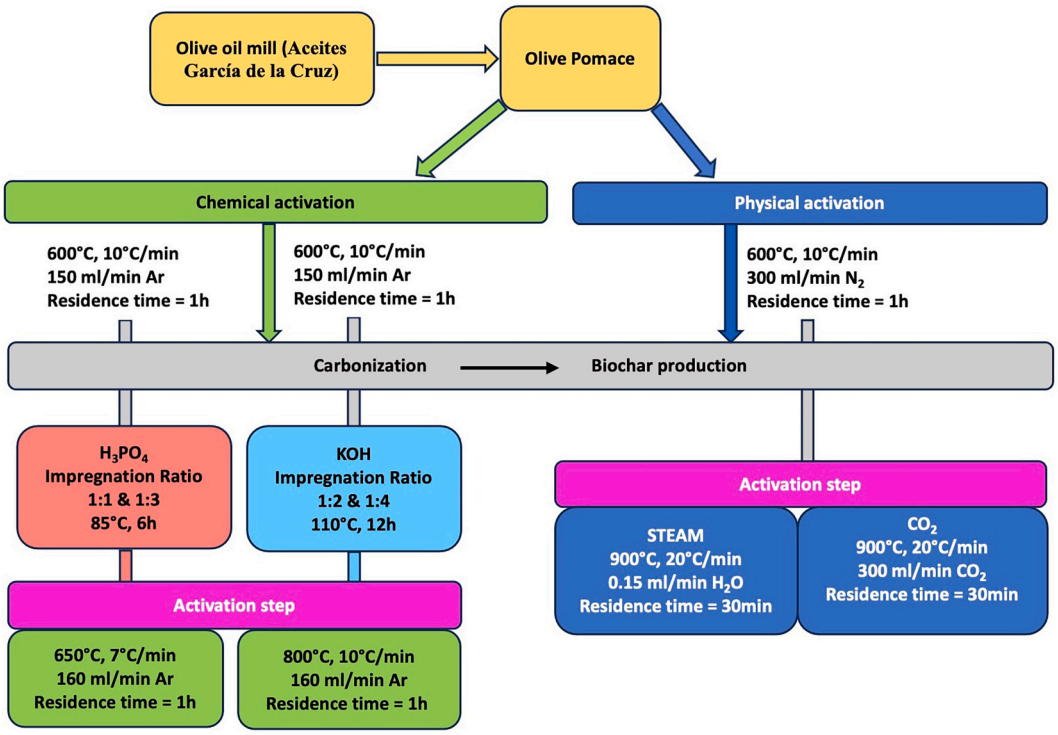

Fig. 1. Olive pomace biochar activation methodologies diagram.

10 °C/min under a constant N_2 flow of 300 ml/min. Then, it was kept at this temperature for one hour. Finally, the resulting biochar was heated to desired activation temperature at a heating rate of 20 °C/min, previously optimized elsewhere [7]. In case of steam activation, operational conditions were set at 900 °C during 30 min at 1 bar of pressure and a constat steam flow of 0.15 ml/min. For CO_2 activation procedure, activation temperature was set at 900 °C during 30 min and 1 bar with a constant CO_2 flow of 300 ml/min. Obtained biochars were named as OP-H_2O and OP-CO_2 for steam and CO_2 activation samples, respectively. The obtained solid or even burn-off yields were calculated using the following equation:

$$Y_{AC,burn-off} = \left((W_{AC} - W_0 A/W_0(1 - A - M)\right)^{*}100\%$$

Where W_{AC} is the weight is the weight of the produced activated carbon, W_0 is the initial weight of the biomass, A is the ash content, and M is the moisture content in the biomass (wt%, dry bases) [32].

2.3. CO_2 adsorption isotherms

The CO_2 adsorption isotherms at 30 °C and 10 bar were performed with a High Pressure Thermobalance (Linseis STA HP/2 HP-TGA DSC) [31]. The equilibrium criterion was set to 0.05 wt% change in 10 min. The initial mass of the sample used for the adsorption isotherms depended on activated carbon yield obtained during activation process. Prior to adsorption the sample was dried in situ at 105 °C for 30 min. Then, the sample was cooled to the measuring temperature, and subsequently, the system was pressurized. The balance purge of the adsorption test was fed with nitrogen and CO_2 flows until 100 % CO_2 atmosphere of 100 ml/min. The maximum adsorption capacity, q (mmol CO_2/g), of each sample was evaluated.

2.4. Sample characterization

The biomass samples underwent characterization through proximate and ultimate analyses. Proximate analysis encompassed the measurement of moisture content, volatile matter, fixed carbon, and ash content. Initially, moisture content determination involved drying OP samples in a convection oven at 110 °C until a constant weight was achieved. Volatile matter content was assessed by measuring weight loss after heating biomass samples to 950 ± 20 °C in an alumina crucible under a nitrogen (N_2) atmosphere, following ASTM D-2013 standards. Ash content determination followed the protocol outlined in Standard E-1755-01, involving heating samples at 575 ± 25 °C for 3 h until reaching constant weight in a muffle furnace. The fixed carbon fraction was computed by deducting the percentages of volatile matter, moisture content, and ash from 100 %. Elemental analysis was conducted using a CHNS-O Elemental Analyzer (Thermo Fisher Scientific, Flash EA 1112).

Thermogravimetric (TGA/DTG) analysis measurements were employed to investigate the thermal decomposition behavior of olive pomace and activated biochars, as well as to validate and compare results obtained through ASTM standard methods regarding moisture content, volatile matter, and fixed carbon. The experiments were conducted utilizing a thermogravimetric analyzer, specifically the Netzsch Thermische Analyze TASC 414/2. Approximately 10 mg of the sample was heated from 25 to 800 °C at a rate of 10 °C/min under a nitrogen (N_2) flow rate of 30 ml/min. Subsequently, the temperature was reduced to 600 °C under an air condition with a flow rate of 70 ml/min to determine ash and fixed carbon content. Ash content was calculated based on the solid residue remaining at the end of the combustion stage, whereas fixed carbon was determined by subtracting the ash content from the solid residue obtained after the TGA test conducted under nitrogen conditions. This technique was used also to determine the ash content in biochars and activated carbons by heating up to 900 °C in an air atmosphere. Differently, TGA/DTG curves of activated biochars were obtained under air conditions with a flow rate of 50 ml/min.

The structure and crystalline phases of the prepared samples (biochars and activated carbons) were determined by a *D8 Advance* diffractometer (Bruker AXS, Germany), operating with a Ni *b*-filtered Cu-Kα radiation (λ = 1.5406 Å) in the 2θ range 5–100° at 40 kV and 40 mA and a scan step of 0.03° s^{-1}. Specifically, phase identification was performed by comparing the position and intensity of the peaks with those of the JCPDS PDF-22004 or International Centre for Diffraction

Data (ICDD) databases using the DIFFRAC.EVA version 6.0 program.

The metal composition of samples was determined by X-ray fluorescence analysis (XRF), using a S8 TIGER spectrometer (Bruker AXS, Germany), equipped with a rhodium anode tube (power 4 kW and 75 μm Be window and LiF 220 crystal analyze). The samples were analyzed as loose powders, considering the emission transitions of copper, zinc and zirconium (Cu-Kα1, Zn-Kα1, Zr-Kα1).

The textural properties of the biochars and activated carbons in terms of surface area, pore volume, and pore size distribution were analyzed and calculated by N_2 adsorption−desorption isotherm measurements at −195.8 °C using Micromeritics ASAP 2020 instrument. Before each measure, the outgassing treatment was performed under a vacuum (5 mmHg) at 250 °C for 12 h. The Brunauer–Emmett–Teller (BET) equation was exploited to calculate the surface area of samples and the total pore volume was obtained from the nitrogen amount adsorbed at a relative pressure of 0.99 (P/P_0). Specifically, the total pore volume (V_T) was calculated through the gas adsorbed amount at 0.99 (p/P0) by the single point method. The micropore surface area (S_{mic}) and the micropore volume (V_{mic}) were obtained by the t-plot method; while the mesopore surface was calculated as the difference to surface area.

The average pore size and pore size distribution were calculated by Barret-Joyner-Halenda (BJH) and Density Functional Theory (DFT) methods respectively; Specifically, for DFT was used the Non-Local Density Functional Theory (NLDFT) using nitrogen adsorption data, assuming a slit pore geometry.

3. Results

3.1. Biochar characterization

Proximate analysis could provide biochar stability and composition. In case of OP analysis, it was found a 7.47 wt%, 9.75 wt%, 70 wt% and 12.78 wt% of ash, moisture, volatile matter and fixed carbon content, respectively. Fixed carbon is one of the indicators to determine the advantages of a biochar.

From an industrial perspective, assessing the carbon yield is crucial to ascertain the feasibility of the material for large-scale applications [33]. The solid yield of obtained samples (Table 1) ranged from 7 to 25 %. Activation procedures reduced the obtained carbon yield compared to carbonized sample (OP-C) due to more processing is needed (activation + washing until neutral pH). However, this reduction was observed less severed for chemical H_3PO_4 and physical steam procedure. It was observed the severity of KOH and CO_2 activation procedures, for which less solid yield was found. The same precursor, when activated by physical activation resulted in a 20 % lower product yield (6.62 %).

Proximate analysis is capable of evaluating both the stability and composition of biochar. Fixed carbon serves as a key indicator in determining the benefits of biochar [34,35]. The decrease of volatile matter is the direct cause of the increase in fixed carbon content, which is consistent with the rule of data in Table 1. This trend was intensified with chemical activation procedures, reducing volatile matter less than 20 wt% and increasing fixed carbon content over 60 wt%. In the case of physical activation, it was found a less reduction of volatile matter while ash content was promoted ranking a 29.5 wt% for OP-CO_2. This increase in ash content could be related to a higher amount of metallic content in produced biochars. Biochar fixed carbon content was closely related to carbon content summarized in Table 2.

The *ultimate analysis* results for determining C, H, N and S percentages (wt%) are summarized in Table 2. According to these data, biochar samples have high amounts of carbon and a lower content of oxygenated compounds. C is the most basic and important element, and its content is generally the highest among all elements [34]. The activated samples have a higher carbon content than raw OP, and also carbonized sample (OP-C), except for the CO_2 physical activated biochar. In case of phosphoric activated biochars, the highest carbon fraction results with higher concentration of the acid in the activation. The opposite effect was observed for KOH activation biochars. The higher oxygen content found for OP-1:4KOH indicate that more oxygenated functional groups are generated and attached to the surface of the biochar. It might be derived from carbohydrate and lignin fractions of lignocellulosic biomass [36]. However, the oxygen content is obtained by difference, it may include unremoved metals, which is consistent with the increase in ash content of the physical activated biochars, OP-H_2O and OP-CO_2 (as observed in Tables 1 and 3). As for H, although it is small (generally accounting for 1 %–3 % of the total mass of biochars), it constitutes important active components such as hydrogen bonded and active functional groups [34]. The reduction in hydrogen content observed during pyrolysis and activation is attributed to the breaking and fragmentation of the weaker bonds within the biomass and biochar carbon structures [36]. The low concentration of nitrogen indicates that the activated biochar is deficient in nitrogen-based functional groups, potentially leading to inadequate absorption of carbon dioxide by the biochar materials through chemisorption [2].

Furthermore, Table 2 reports the O/C ratios. The decrease in these ratios compared to the original biomass indicates the development of aromaticity and hydrophobicity in the structure of the activated biochars, due to the removal of oxygen from within the material. Specifically, activated biochars with an O/C value lower than 0.4 exhibit greater stability [37,38].

The presence of metals in biomass and activated biochars was observed through XRF analysis (Table 3) and could exist inherently in different forms. Its presence could be associated with biomass polymers by binding with oxygen-containing functional groups in polymers such as carboxyl groups in cellulose or phenolic groups in lignin [39]. Raw OP was found enriched in metal content, especially potassium (K) (8.15 wt %). K could act as a catalyst during decarbonylation and decarboxylation of the pyrolysis vapors [40]. The content of this metal was reduced after chemical activation procedures, especially in OP-1:3H_3PO_4 sample (0.88 wt%). This suggests that K are present in large as water-soluble salt [41]. In the case of physical activated biochars, K was fixed and enriched

Table 1
Solid carbon yields and proximate analysis data.

Sample	Burn-off Yield (wt%)	Proximate analysis (wt%)			
		Moisture	Volatile matter	Ash	Fixed Carbon*diff
OP	–	9.75	70	7.47	12.78
OP-C	27.83	6.37	62.60	11.62	19.41
OP-1:1H_3PO_4	21.95	5.29	17.86	3.76	73.09
OP-1:3H_3PO_4	21.93	3.93	16.90	5.64	73.53
OP-1:2KOH	14.04	10.42	14.67	4.97	69.94
OP-1:4KOH	7.66	10.97	22.03	4.35	62.65
OP-H_2O	23.63	5.98	40.22	14.86	38.94
OP-CO_2	6.62	7.53	44.34	29.51	18.62

Table 2
Elemental analysis of different activated biochars.

Sample	Ultimate analysis (wt%)*daf					
	N	C	H	S	O*diff	O/C
OP	1.47	52.20	6.91	0.15	39.27	0.75
OP-C	2.66	71.38	2.53	–	23.42	0.33
OP-1:1H_3PO_4	2.60	79.78	2.36	–	15.27	0.19
OP-1:3H_3PO_4	2.96	85.65	2.66	–	8.73	0.10
OP-1:2KOH	0.81	82.69	0.80	–	15.70	0.19
OP-1:4KOH	1.23	76.43	0.85	–	21.50	0.28
OP-H_2O	2.25	69.71	0.86	0.07	27.11	0.39
OP-CO_2	4.78	61.05	1.47	0.24	32.46	0.53

*daf: dry and ash free basis: O^{diff}: % of oxygen calculated from the difference in C, H, N and S.

Table 3
X-ray fluorescence analysis of different activated biochars.

	Mineral content (wt%)							
Sample	Mg	P	S	Cl	K	Ca	Fe	Sr
OP	0.06	0.28	0.39	0.73	8.15	1.3	0.03	0.03
OP-C	0.17	0.89	0.17	1.57	21.27	4.2	0.28	0.09
OP-1:1H_3PO_4	0.24	2.29	0.16	0.40	1.22	4.05	0.13	0.09
OP-1:3H_3PO_4	0.25	3.99	0.14	0.15	0.88	3.6	0.12	0.09
OP-1:2KOH	0.18	0.53	–	0.10	6.94	2.62	–	0.05
OP-1:4KOH	0.10	0.35	0.14	0.18	2.79	1.59	0.79	0.03
OP-H_2O	0.28	1.03	0.26	2.01	24.29	4.99	0.12	0.12
OP-CO_2	0.95	2.26	0.31	2.94	36.99	8.06	0.15	0.20

due to severe procedure temperature up to 20 wt% (OP-CO_2 contained approx. 37 wt% of K). Same trend was observed for carbonized sample. However, phosphorus content increase as expected with H_3PO_4 activation process, up to 4 wt% for high acid concentration sample. Apart from alkali metals, alkaline earth metals like calcium (Ca) became significant in the activated biochars samples. Most of inherent metals presents in raw OP during carbonization were retained in the carbonizes structure as observed in Table 3.

The thermal decomposition behavior of olive pomace (OP) was investigated using thermogravimetric analysis (TGA) and derivative thermogravimetric analysis (DTG). The thermogravimetric profile is shown in Fig. 2. Five distinct stages were observed: four in a nitrogen atmosphere and the final one in an air atmosphere. Specifically, the first stage, occurring between 100 and 120 °C, was attributed to moisture loss. The second stage, between 140 and 200 °C and 250–400 °C, was due to the decomposition of various compounds, such as hemicellulose, cellulose, and the degradation of xylose polymers. The mass loss in the third stage was attributed to lignin decomposition, which takes place at higher temperatures within the range of 500–600 °C. The fourth stage, extending up to 800 °C, corresponds to char formation and stabilization [11,42,43]. Finally, the last stage, recorded in the presence of air, was due to carbon oxidation. This conclusion is clearly supported by both the TG and DTG profiles, as indicated by a peak corresponding to the burning of char.

The TGA/DTG curves of the activated carbons are shown in Fig. 3. For all samples, on both curves, the initial weight loss up to 150 °C mainly corresponds to moisture. The weight loss observed between 200 and 650 °C exhibited exothermic effects and decomposition rates (DTG curves) ranging from 458 °C (OP-1:2KOH) to 513 °C (OP-1:3H_3PO_4), associated with the decomposition of organic compounds (decarboxylation and dehydration) [44] and the degradation of the carbon structure. Particularly, samples activated with potassium hydroxide (OP-1:2KOH and OP-1:4KOH) exhibited the steepest slope in thermal decomposition, which can be attributed to a stronger interaction with the chemical agent, resulting in the highest total pore volume (Table 4) [11].

The XRD patterns of the biomass, char, and activated carbons are shown in Fig. 4. Olive pomace biomass exhibits a characteristic cellulose peak at $2\theta = 20°$ and another peak at $2\theta = 29.3°$, corresponding to the crystalline phase of calcite [11,42–45]. The presence of the latter compound is also validated by XRF data. The XRD spectra of all carbonaceous structures, specifically char and activated carbons, display two broad peaks, indicating a typical amorphous carbon structure at 2θ of 24° and 43°, which correspond to the (002) and (100) planes of graphite-like reflections, signifying graphitic ordering in the molecular structure [11,42,43]. In particular, the diffractograms of OP-C, OP-CO_2, and OP-H_2O show, when compared with the patterns reported in the International Centre for Diffraction Data (ICDD), the presence of Potassium Hydrogen Carbonate, $KHCO_3$ (PDF 70–1168), Potassium Hydrogen Carbonate Hydrate, $K_4H_2(CO_3)_3$*1.5H_2O (PDF 20–0886) and Calcite. The calcite peaks are partly masked by the high crystallinity of $KHCO_3$ and $K_4H_2(CO_3)_3$*1.5H_2O [11]. Chemically activated carbons, both acidic and basic, do not show the presence of these compounds, except for a small amount of calcite in the KOH-activated biochars. This suggests that the activation process significantly reduces the presence of these mineral impurities. The results of these diffractometric measurements align with the XRF data (Table 3), which shows a high concentration of calcium and potassium, derived from the crystalline structures mentioned, in the raw biomass, char, and physically activated carbons.

The nitrogen sorption behavior of activated carbons derived from olive pomace, using both physical and chemical activation methods, is

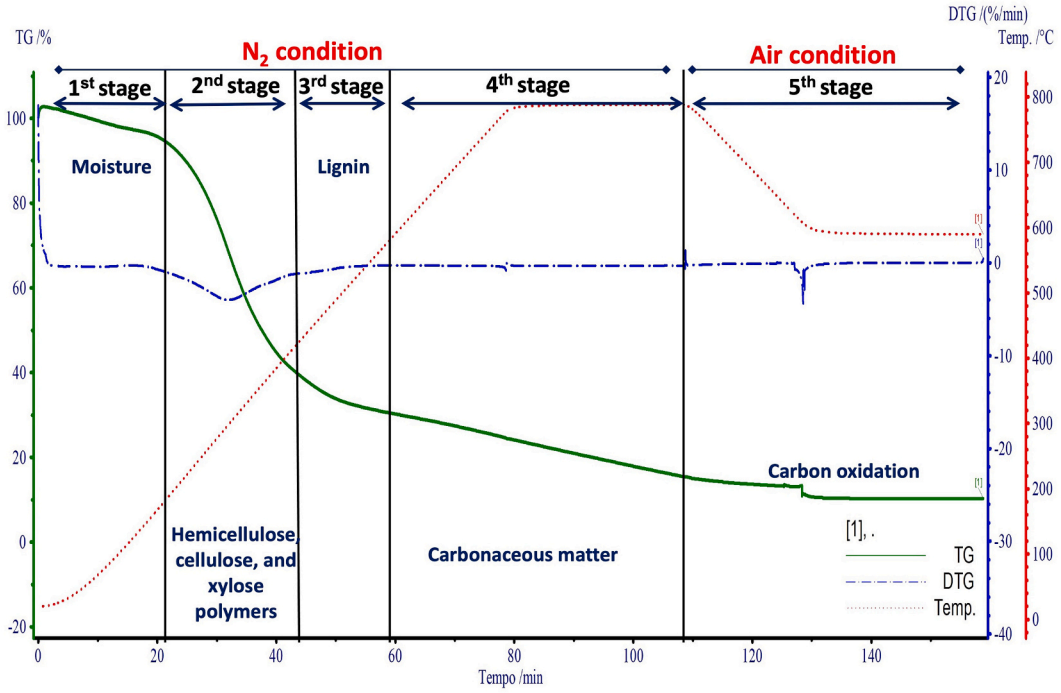

Fig. 2. TGA and DTG curves of Olive Pomace.

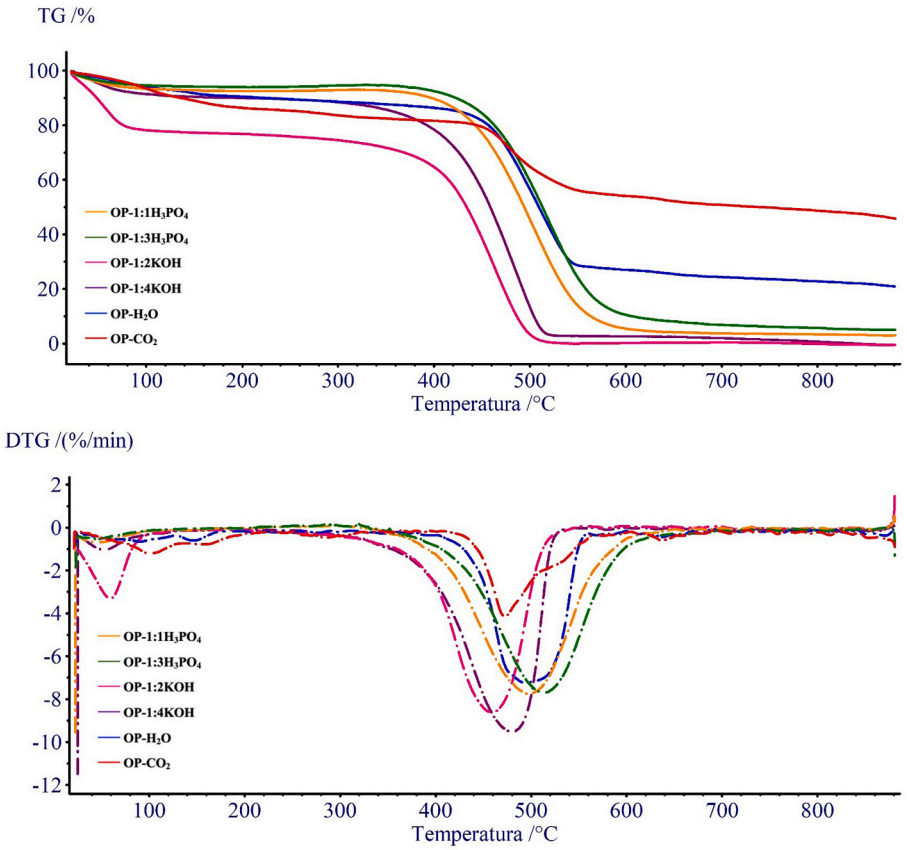

Fig. 3. TGA and DTG curves of activated biochars.

Table 4
Textural parameters of activated carbons.

Sample	Surface area m^2/g			S_{mic}/S %	Pore volume cm^3/g		V_{mic}/V_T %	[d]Average pore width nm	[c]Average pore width nm
	[a]S	[b]S_{mic}	S_{meso}		[c]V_T	[b]V_{mic}			
OP-1:1H_3PO_4	17.39 ± 0.59	6.44	10.95	37.1	0.016	0.006	38.1	55.619	2.734
OP-1:3H_3PO_4	18.84 ± 0.22	7.28	11.56	38.6	0.015	0.007	45.9	49.323	2.378
OP-1:2KOH	986.80 ± 2.99	890.85	95.95	90.3	0.397	0.342	86.2	4.518	1.663
OP-1:4KOH	985.51 ± 3.97	859.64	125.87	87.2	0.446	0.331	74.2	9.017	1.389
OP-H_2O	19.69 ± 0.23	11.18	8.51	39.8	0.010	0.005	31.2	42.814	2.193
OP-CO_2	129.64 ± 1.48	51.66	77.99	56.8	0.074	0.023	44.9	10.601	2.810

[a]BET method; [b]t-plot method; [c]Single point method; [d]BJH method;

summarized in Table 4. The biochar activation process is critical for enhancing surface properties and, consequently, improving CO_2 adsorption capacity. Textural characteristics such as surface area (S), micropore area (S_{mic}), mesopore area (S_{meso}), total pore volume (VT), micropore volume (V_{mic}), and pore width are detailed in Table 4. The correlation between the activation method used and porosity development can be inferred from the data, particularly in the samples chemically activated with KOH, and to a lesser extent, the sample physically activated with CO_2.

Notably, both biochars prepared with KOH at ratios of 1:2 and 1:4 (OP-1:2KOH, OP-1:4KOH) showed a significant increase in surface area (approximately 986.90 m^2/g) compared to the pristine OP biochar (1–8 m^2/g as per literature values) [11,46,47]. Similarly, the enhancement of the microporous structure was confirmed by the Smic/S and Vmic/VT ratios reported in Table 4. A similar, though less pronounced, effect was observed with CO_2 physical activation, resulting in a surface area of 129.64 m^2/g. By contrast, steam activation and chemical activation with H_3PO_4 at all ratios produced only slight increases in surface area.

This experimental evidence is further supported by the nitrogen adsorption-desorption isotherms shown in Fig. 5. The OP-1:2KOH and OP-1:4KOH samples exhibited typical Type I isotherm curves at relative pressures up to 0.45, indicating a microporous structure. At higher relative pressures, however, they displayed a hysteresis loop characteristic of Type IV isotherms, suggesting the presence of mesopores as well [2,11,28,48].

Generally, Type I isotherms display sharp adsorption at low pressure

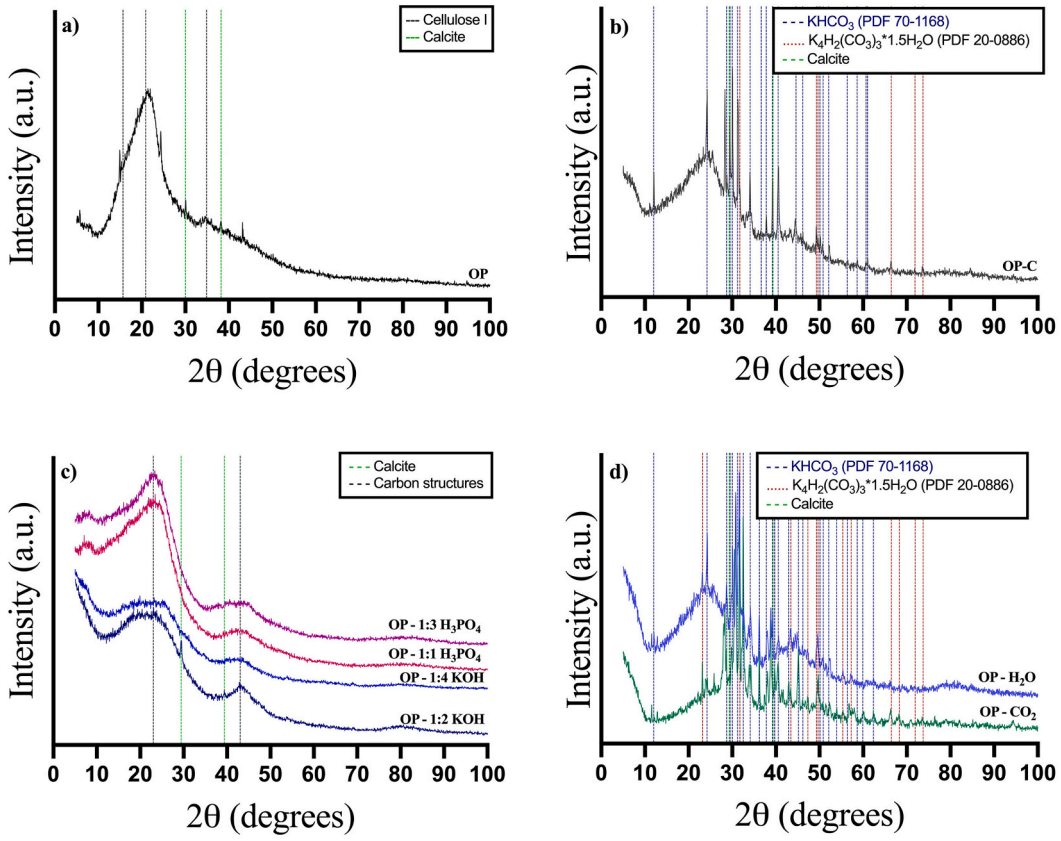

Fig. 4. XRD patterns of: a) OP; b) OP-C; c) Activated carbons by chemical treatment; d) Activated carbons by physical treatment.

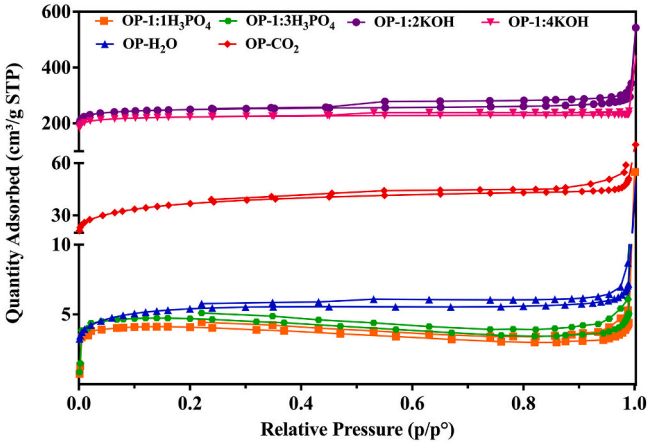

Fig. 5. Nitrogen adsorption-desorption isotherms at temperature − 195.8 °C of olive pomace activated.

values (P/P_o), due to strong adsorbent-adsorbate interactions in narrow micropores, facilitating micropore filling. Once a specific adsorption threshold is reached, further increases in P/P_o lead to only minor additional adsorption [11,28]. It should also be noted that, in the case of KOH activation, the higher KOH ratio (1:4) for the OP-1:4KOH sample resulted in a surface area similar to the lower ratio (1:2), but with a different pore distribution. This is presumably due to both the characteristics of the starting biomass and the fact that a high quantity of oxidizing agent partly led to the explosion and collapse of the microporous structure, as reported in Table 4.

In contrast, the OP-1:H_3PO_4, OP-1:3H_3PO_4, and OP-H_2O carbons exhibited relatively poor porous structures, as indicated by their low BET surface areas (17.39–19.69 m^2/g). Despite the use of two different activation ratios (1:1 and 1:3) for H_3PO_4 activation, this did not result in significant surface area development. This may be attributed to residual P-activator components, as confirmed by XRF analysis (Table 3), or to pore collapse and shrinkage. In the case of physical activation, the low surface area could be due to incomplete carbonization of the starting biomass and the presence of undesirable compounds (e.g., $KHCO_3$), as observed in the XRD analysis (Fig. 4), which may have blocked the pores.

Pore size distribution analysis confirmed the mixed presence of micro, *meso*, and macropores in the activated carbons derived from olive pomace. DFT-calculated pore size distributions and percentages, reported in Fig. 6 and Table 5, showed a higher percentage of micropores in OP-1:2KOH and OP-1:4KOH (73.31 % and 40.42 %, respectively).

Additionally, analyses using the BJH method aligned well with the DFT calculations. The contribution of micropore surface area ranged from 87.2 % to 90.3 % in the KOH-activated samples, whereas it was much lower (37.1–39.8 %) in the samples activated with acidic or steam methods.

Furthermore, chemical activation with KOH resulted in the highest micropore volume (0.342 cm^3/g), while other activation methods produced significantly lower micropore volumes (0.006 cm^3/g). In other activated biochars meso- and macropores dominated the structure, explaining their relatively low surface area values.

The morphologies of carbonized OP char and activated biochars (OP-1:1H_3PO_4, OP-1:3H_3PO_4, OP-1:2KOH, OP-1:4KOH, OP-H_2O and OP-CO_2) by HRSEM are demonstrated in Fig. 7. After carbonizing OP, the porosity of the biochars was developed with the activation procedures, which is consistent with previous textural results (Tables 4 and 5). From obtained XRD patterns and HRSEM images it was corroborated the amorphous carbon structure. The physical activation of biochar (steam and CO_2) mainly results in tubular pore structure, while chemical

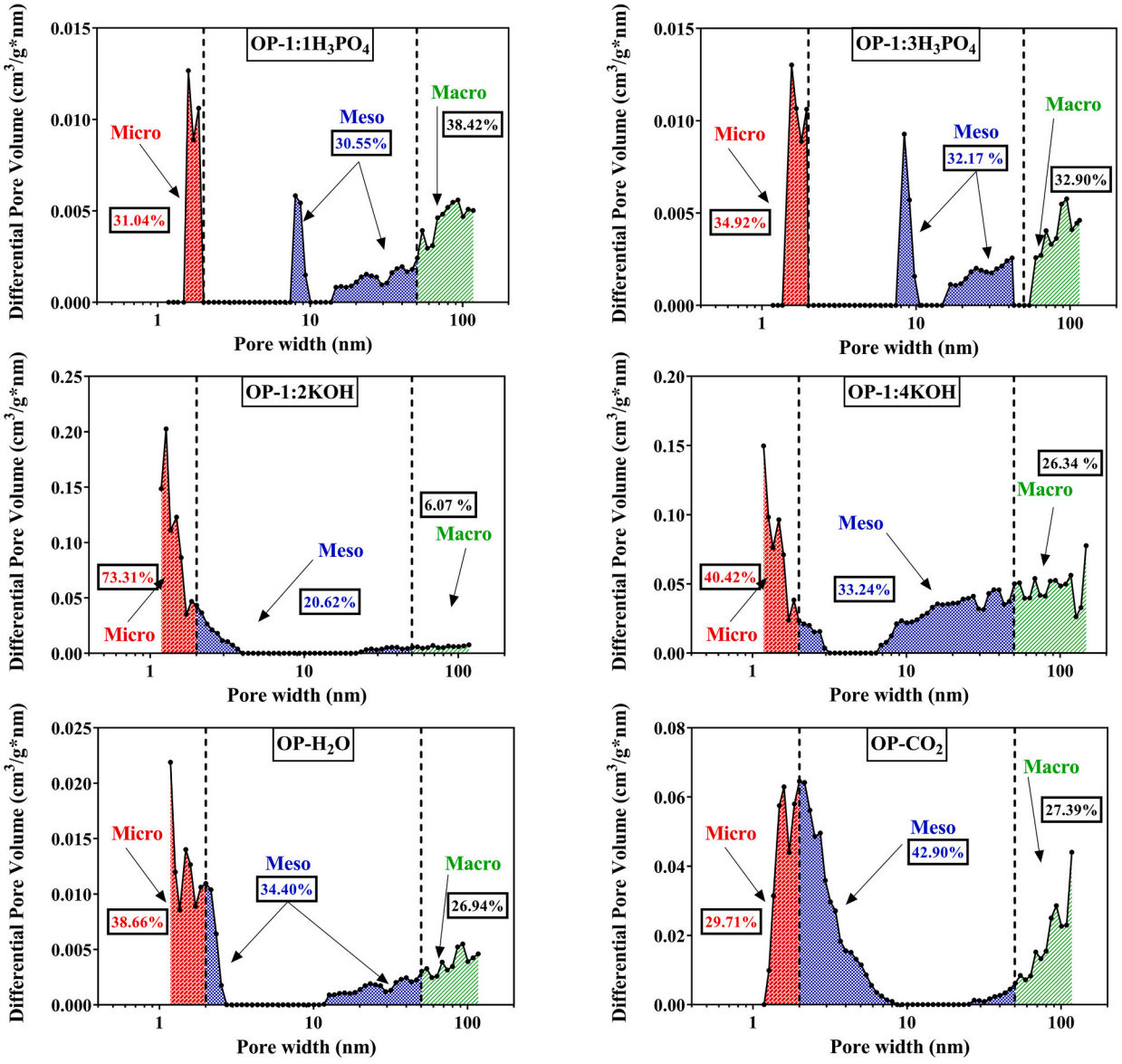

Fig. 6. DFT pore size distribution.

Table 5
Pore size distribution (%).

Sample	Micro (%)	Meso (%)	Macro (%)
OP-1:1H_3PO_4	31.04	30.55	38.42
OP-1:3H_3PO_4	34.92	32.17	32.90
OP-1:2KOH	73.31	20.62	6.07
OP-1:4KOH	40.42	33.24	26.34
OP-H_2O	38.66	34.40	26.94
OP-CO_2	29.71	42.90	27.39

activation produces pore expansion and corrosion [2,49,50]. However, a highly porous structure was obtained especially for OP-1:2KOH (Fig. 7D), OP-1:4KOH (Fig. 7E) and OP-CO_2 (Fig. 7G). These results were also coherent with previous DFT pores size distribution for which KOH activation procedure yielded the highest volume of micropores.

3.2. Biochar CO_2 adsorption capacity

The CO_2 adsorption behavior of biochar at 30 °C and 10 bar is presented in Fig. 7. The Ideal Adsorbed Solution Theory (IAST), which is based on Langmuir fit CO_2 and N_2 isothermal adsorption, serves as a key criterion for evaluating biochar's CO_2 adsorption capacity [7,31].

As illustrated in Fig. 8, the CO_2 adsorption capacities of the various activated biochars tested show a generally consistent trend. Additionally, the CO_2 adsorption capacities of raw olive pomace (OP) and its carbonized form without further activation (OP-C) were evaluated for comparison, with the raw OP showing no CO_2 uptake.

The pore structure and surface chemistry of biochar materials are not well-developed, which hinders CO_2 capture. To enhance CO_2 adsorption capacities, modifications such as acid or alkaline activation, physical activation, heteroatom doping, or metal impregnation are necessary [51]. Selecting the appropriate activation conditions such as the modifier, treatment temperature, and duration is crucial because these factors significantly influence the effectiveness of the modification. Activated carbons typically show higher CO_2 adsorption capacities than biochar due to the improved textural properties and surface chemistry that result from activation treatments, which enhances CO_2 adsorption potential. The mechanism of CO_2 capture by activated carbon involves both physical and chemical adsorption processes. Physical adsorption, driven by van der Waals forces and pore filling, is significantly influenced by

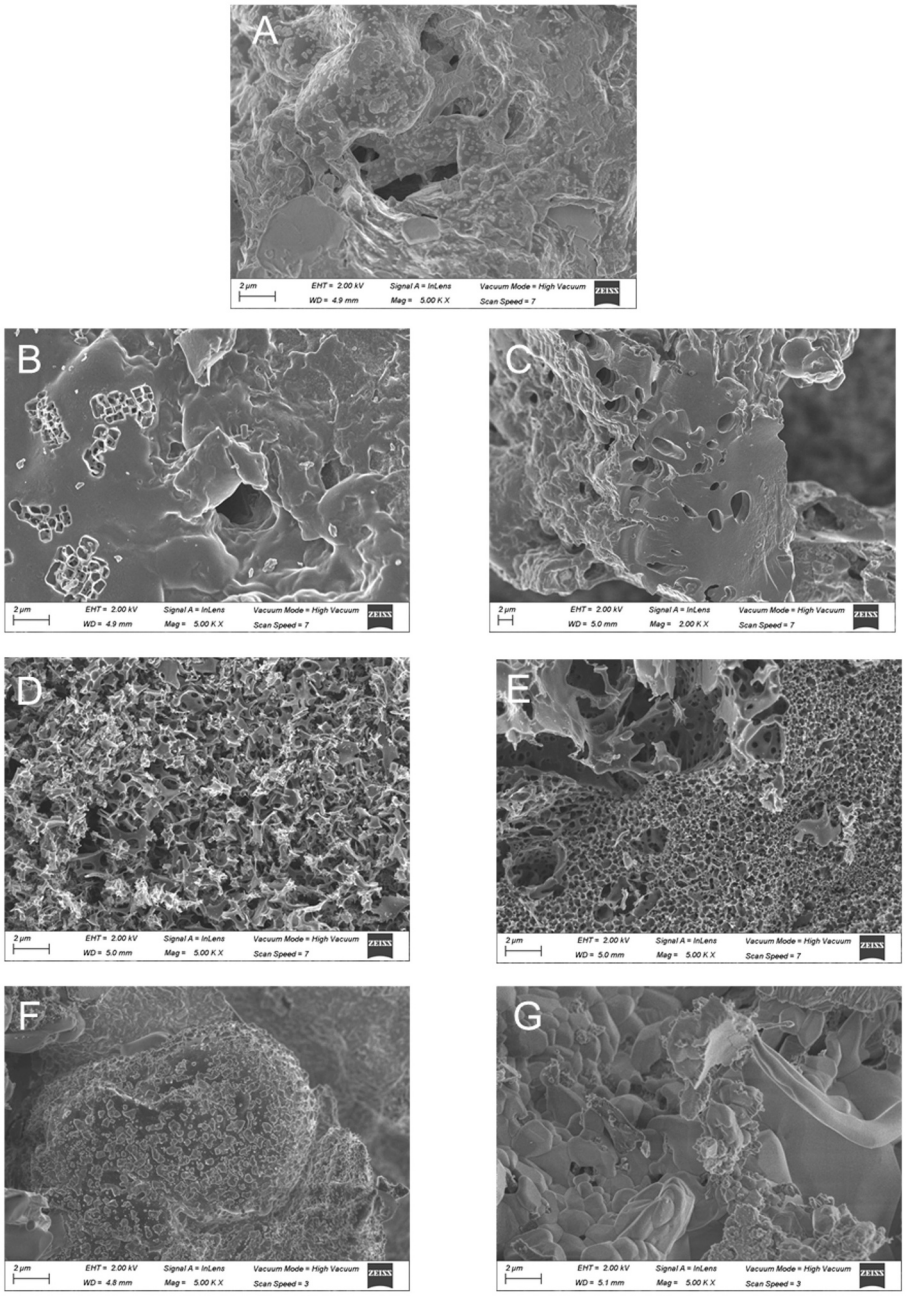

Fig. 7. HRSEM micrographs of carbonized biochar, OP-C (A), and activated biochars: (B) OP-1:1H_3PO_4, (C) OP-1:3H_3PO_4, (D) OP-1:2KOH, (E) OP-1:4KOH, (F) OP-H_2O and (G) OP-CO_2.

temperature, while chemical adsorption involves the formation of chemical bonds between CO_2 and the adsorbent, with Lewis acid-base interactions and hydrogen bonding playing essential roles.

Among the synthesized activated biochars, not all activation methods improved adsorption capacity. Chemical activation methods led to greater CO_2 capture compared to physical activation.

For example, KOH chemical activation significantly enhanced CO_2 adsorption, with capacities of 3.04 mmol/g and 2.16 mmol/g for OP-1:2KOH and OP-1:4KOH, respectively, at 30 °C and 1 bar. This improvement is closely related to the micro and mesopore distribution of the samples (40.42–73.31 % micropores for OP-1:2KOH and 20.62–33.24 % for OP-1:4KOH). The redox reaction between KOH and carbon precursors begins at around 400 °C, leading to the formation of K_2CO_3. At around 600 °C, KOH fully converts to K_2CO_3, and when temperatures exceed 700 °C, K_2CO_3 decomposes into CO_2 and K_2O. At these high temperatures, both K_2CO_3 and K_2O can be further reduced to potassium (K), which vaporizes and intercalates into the carbon lattice, promoting micropore development [51]. KOH activation is assumed to enhance CO_2 capture due to the highest volume of micropores (0.342 cm^3/g).

The acidic nature of CO_2 means that introducing Lewis base sites on the surface of carbon materials enhances CO_2 capture. This is attributed to the chemisorption effect between the adsorbents and CO_2, where hydrogen bonds form between CO_2 molecules and –OH groups introduced during KOH activation. Further analysis indicates that hydrogen bonding lowers the binding energy between the adsorbents and CO_2, significantly improving CO_2 adsorption [2,17,51]. The adsorption capacity of KOH-activated biochars was found to rapidly increase as the CO_2 concentration rose, with an uptake of nearly 2 mmol/g of adsorbate at 25 % *v*/v CO_2 (Fig. 8B).

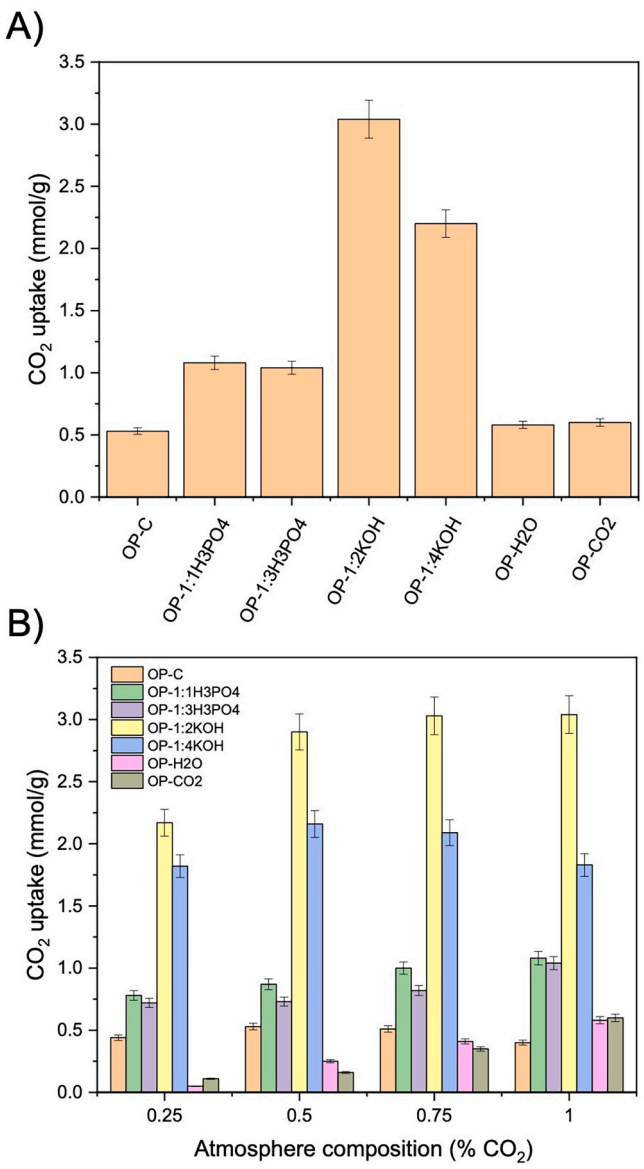

Fig. 8. Biochar CO_2 capture capacities tested: A) net CO_2 uptake (mmol/g) and B) capture CO_2 evolution as increase gas atmosphere percentage.

Although lower than KOH-activated biochars, the CO_2 adsorption capacity of H_3PO_4-activated biochars can be attributed to a favorable pore distribution between micro and mesopores (Table 5), low O/C ratios (0.10–0.19, Table 2), and a higher nitrogen content (2.60–2.96 %, Table 2), which suggests nitrogen functionalization. These factors appear to positively influence CO_2 adsorption [2,52].

Indeed, the CO_2 adsorption mechanism is not determined by a single factor but rather by the synergistic effect of several factors, including surface area, elemental composition, and surface chemical properties such as acidity, hydrophobicity, and polarity of the activated materials [2,53]. The O/C ratio (Table 2) reflects the polarity and hydrophilicity of the activated biochars: low O/C ratios indicate high aromatization and hydrophobicity, which may enhance CO_2 adsorption [54]. Conversely, a high O/C ratio indicates the presence of oxygen-containing functional groups, increasing hydrophilicity and polarity, favoring water vapor over CO_2 for adsorption sites [55].

However, the reduced performance of H_3PO_4-activated biochars compared to KOH-activated ones may be due to the increased surface acidity caused by the introduction of P-containing functional groups, as seen in the XRF data (Table 3). Since CO_2 is an acidic molecule, the acidic PxOy groups generated from H_3PO_4 activation are detrimental to CO_2 chemisorption in carbon materials [17,51]. H_3PO_4-activated biochars reached their micropore saturation point at 25 % *v*/v CO_2. As seen in Fig. 8B, the adsorption rate slightly increased with higher CO_2 concentrations.

On the other hand, physical activation did not significantly improve CO_2 capture, despite promoting a microporous and mesoporous structure in OP-CO_2 (Table 5). Although physical activation can improve pore structure, other factors, such as surface functionality, also play a role in CO_2 capture. The poor performance of physically activated biochars may be related to the high ash content and low fixed carbon content (Table 1). The enrichment of potassium (K) up to 20 wt% in OP-CO_2 biochar (Table 3) may explain some level of adsorption through chemisorption interactions between K-surface atom with the acidic CO_2. The presence of K+ ions promote CO_2 adsorption via electrostatic interactions [56].

Chemical activation, particularly with KOH, produced the highest specific surface area and micropore volume, resulting in superior CO_2 adsorption performance. When comparing the CO_2 adsorption capacity of OP biochar synthesized with a 1:2 KOH ratio to previous studies (Table 6), it becomes clear that its performance is comparable to that of commercially activated carbon (Sigma-Aldrich®) and other biochars derived from various biomass wastes.

In summary, the results show that the CO_2 adsorption capacities of the four activated biochars tested followed the order: KOH > H_3PO_4 > CO_2 > H_2O under the conditions of 30 °C and 10 bar. Thus, the best activation method was the chemical basic treatment, which led to more microporous structures and, therefore, superior adsorption properties.

4. Conclusion

The effect of activation conditions (both chemical and physical) on activated biochars derived from olive pomace was evaluated in terms of CO_2 uptake, physicochemical, and textural properties. The results indicate that the CO_2 adsorption mechanism is not determined by a single factor but rather by the synergistic effect of several factors, including surface area, elemental composition, and surface chemical properties such as acidity, hydrophobicity, and polarity of the activated materials.

Chemical activation, in particular, resulted in more microporous structures, leading to improved CO_2 adsorption capacity. Using the chemical KOH activation method, CO_2 adsorption was enhanced to 3.04 mmol/g and 2.16 mmol/g with a solid yield of 14.1 % and 4.6 % for OP-1:2KOH and OP-1:4KOH, respectively. It was demonstrated that textural and adsorption properties could be improved in OP biochars without the need for highly concentrated KOH activation procedures. Textural analysis revealed that KOH chemical activation primarily promoted micropore development, while other activation methods produced both

Table 6
CO_2 adsoprtion performance of commercial and KOH activated biochars comparison.

	S_{BET} (m^2/g)	CO_2 adsorption (mmol/g)	Reference
OP-1:2KOH	986	3.1	This study
Activated carbon (Sigma Aldrich®)	850	4.9	[7]
Camphor leaves	1146	3.74	[17]
Chicken manure waste	22.22	1.95	
Olive mill waste	1036	3.52	
Rice husk	1162	1.8	
Water chestnut shell	1517	2.95	
Sargassum	291.8	1.05	
Starch	714	2.8	[16]
Coffee grounds	876	3	
Lignin waste	2750	2.4	
Garlic peel	1206	2.82	

micropores and mesopores. In contrast, acid and physical activation of biochar reduced CO_2 adsorption due to changes in the internal structure. In conclusion, olive pomace shows great promise as a cost-effective precursor for creating biochar adsorbents, especially when KOH is used as the activating agent, resulting in significant adsorption capacities.

CRediT authorship contribution statement

A. Alcazar-Ruiz: Writing – original draft, Methodology, Investigation, Data curation, Conceptualization. **S. Maisano:** Writing – review & editing, Validation, Supervision, Methodology, Conceptualization. **V. Chiodo:** Writing – original draft, Validation, Supervision, Conceptualization. **F. Urbani:** Writing – original draft, Validation, Data curation, Conceptualization. **F. Dorado:** Writing – review & editing, Supervision, Funding acquisition, Formal analysis. **L. Sanchez-Silva:** Writing – review & editing, Validation, Supervision, Resources, Conceptualization.

Declaration of competing interest

The authors declare that they have no known competing financial interests or personal relationships that could have appeared to influence the work reported in this paper.

Data availability

Data will be made available on request.

References

[1] T.M.L. Wigley, The pre-industrial carbon dioxide level, Clim. Chang. 5 (1983) 315–320, https://doi.org/10.1007/BF02423528.

[2] C. Zhang, Y. Ji, C. Li, Y. Zhang, S. Sun, Y. Xu, L. Jliang, C. Wu, The application of biochar for CO_2 capture: influence of biochar preparation and CO_2 capture reactors, Ind. Eng. Chem. Res. 62 (2023) 17168–17181, https://doi.org/10.1021/acs.iecr.3c00445.

[3] M. Pardakhti, T. Jafari, Z. Tobin, B. Dutta, E. Moharreri, N.S. Shemshaki, S. Suib, R. Srivastava, Trends in solid adsorbent materials development for CO_2 capture, ACS Appl. Mater. Interfaces 11 (2011) 34533–34559, https://doi.org/10.1021/acsami.9b08487.

[4] H. Demir, G.O. Aksu, H.C. Gulbalkan, S. Keskin, MOF membranes for CO_2 capture: past, present and future, Carbon Capture Sci. Technol. 2 (2022) 100026, https://doi.org/10.1016/j.ccst.2021.100026.

[5] S. Kumar, R. Srivastava, J. Koh, Utilization of zeolites as CO_2 capturing agents: advances and future perspectives, J. CO2. Util. 41 (2020) 101251, https://doi.org/10.1016/J.JCOU.2020.101251.

[6] F. Qin, C. Zhang, G. Zeng, D. Huang, X. Tan, A. Duan, Lignocellulosic biomass carbonization for biochar production and characterization of biochar reactivity, Renew. Sust. Energ. Rev. 157 (2022) 112056, https://doi.org/10.1016/j.rser.2021.112056.

[7] M. Puig-Gamero, A. Esteban-Arranz, L. Sanchez-Silva, P. Sanchez, Obtaining activated biochar from olive stone using a bench scale high-pressure thermobalance, J. Environ. Chem. Eng. 9 (2021) 105374, https://doi.org/10.1016/J.JECE.2021.105374.

[8] A.V. Bridgwater, D. Meier, D. Radlein, An overview of fast pyrolysis of biomass, Org. Geochem. 30 (1999) 1479–1493, https://doi.org/10.1016/S0146-6380(99)00120-5.

[9] A. Alcazar-Ruiz, R. Garcia-Carpintero, F. Dorado, L. Sanchez- Silva, valorization of olive oil industry subproducts: ash and olive pomace fast pyrolysis, Food Bioprod. Process. 125 (2021) 37–45, https://doi.org/10.1016/j.fbp.2020.10.011.

[10] J. Saleem, U.B. Shahid, M. Hijab, H. Mackey, G. McKay, Production and applications of activated carbons as adsorbents from olive stones, Biomass Convers. Biorefinery 9 (2019) 775–802, https://doi.org/10.1007/s13399-019-00473-7.

[11] K. Kiełbasa, Ş. Bayar, E.A. Varol, J. Sreńscek-Nazzal, M. Bosacka, B. Michalkiewicz, Thermochemical conversion of lignocellulosic biomass - olive pomace - into activated biocarbon for CO_2 adsorption, Ind. Crop. Prod. 187 (2022) 115416, https://doi.org/10.1016/j.indcrop.2022.115416.

[12] B. Sajjadi, W.Y. Chen, N.O. Egiebor, A comprehensive review on physical activation of biochar for energy and environmental applications, Rev. Chem. Eng. 35 (2019) 735–776, https://doi.org/10.1515/revce-2017-0113.

[13] C. Di Stasi, D. Alvira, G. Greco, B. González, J.J. Manyà, Physically activated wheat straw-derived biochar for biomass pyrolysis vapors upgrading with high resistance against coke deactivation, Fuel 255 (2019) 115807, https://doi.org/10.1016/J.FUEL.2019.115807.

[14] X. Yuan, Y. Shen, P.A. Withana, O. Mašek, C.S.K. Lin, S. You, F.M.G. Tack, Y.S. Ok, Thermochemical upcycling of food waste into engineered biochar for energy and environmental applications: a critical review, Chem. Eng. J. 469 (2023) 143783, https://doi.org/10.1016/J.CEJ.2023.143783.

[15] N.A. Rashidi, S. Yusup, Potential of palm kernel shell as activated carbon precursors through single stage activation technique for carbon dioxide adsorption, J. Clean. Prod. 168 (2017) 474–486, https://doi.org/10.1016/j.jclepro.2017.09.045.

[16] B. Dziejarski, J. Serafin, K. Andersson, R. Krzyżyńska, CO_2 capture materials: a review of current trends and future challenges, Mater. Today Sustain. 24 (2023) 100483, https://doi.org/10.1016/j.mtsust.2023.100483.

[17] C. Goel, S. Mohan, P. Dinesha, CO_2 capture by adsorption on biomass-derived activated char: a review, Sci. Total Environ. 798 (2021) 149296, https://doi.org/10.1016/j.scitotenv.2021.149296.

[18] K. Malini, D. Selvakumar, N.S. Kumar, Activated carbon from biomass: preparation, factors improving basicity and surface properties for enhanced CO_2 capture capacity – a review, J. CO2. Util. 63 (2023) 102318, https://doi.org/10.1016/J.JCOU.2022.102318.

[19] S. Acevedo, L. Giraldo, J.C. Moreno-Piraján, Materiais carbonosos preparados a partir de Cuesco de Palma en a adsorção de CO_2. Caracterização elementar, proximal y morfológica, Rev. Colomb. Química 50 (2021) 30–39, https://doi.org/10.15446/rev.colomb.quim.v50n2.95020.

[20] Q. Cao, K.C. Xie, Y.K. Lv, W.R. Bao, Process effects on activated carbon with large specific surface area from corn cob, Bioresour. Technol. 97 (2006) 110–115, https://doi.org/10.1016/J.BIORTECH.2005.02.026.

[21] S. Li, X. Tan, H. Li, Y. Gao, Q. Wang, G. Li, M. Guo, Investigation on pore structure regulation of activated carbon derived from sargassum and its application in supercapacitor, Sci. Rep. 12 (2022) 1–17, https://doi.org/10.1038/s41598-022-14214-w.

[22] D. Bergna, T. Hu, H. Prokkola, H. Romar, U. Lassi, Effect of some process parameters on the main properties of activated carbon produced from peat in a lab-scale process, Waste Biomass Valoriz. 11 (2020) 2837–2848, https://doi.org/10.1007/s12649-019-00584-2.

[23] W. Deng, M. Hu, S. Xu, M. Hu, G. Chen, H. Ji, P. Zhou, X. Su, Pyrolysis of sludge briquettes for the preparation of cylindrical-shaped biochar and comparison between CO_2 and steam activation, Fuel 338 (2023) 127317, https://doi.org/10.1016/j.fuel.2022.127317.

[24] R. Pedicini, S. Maisano, V. Chiodo, G. Conte, A. Policicchio, R.G. Agostino, Posidonia Oceanica and Wood chips activated carbon as interesting materials for hydrogen storage, Int. J. Hydrog. Energy 45 (2020) 14038–14047, https://doi.org/10.1016/j.ijhydene.2020.03.130.

[25] S. Maisano, F. Urbani, N. Mondello, V. Chiodo, Catalytic pyrolysis of Mediterranean sea plant for bio-oil production, Int. J. Hydrog. Energy 42 (2017) 28082–28092, https://doi.org/10.1016/j.ijhydene.2017.07.124.

[26] Y. Sait, Y. Derya, Preparation and characterization of activated carbons from Paulownia wood by chemical activation with H_3PO_4, J. Taiwan Inst. Chem. Eng. 53 (2015) 122–131, https://doi.org/10.1016/j.jtice.2015.02.032.

[27] S. Zuo, J. Yang, J. Liu, Effects of the heating history of impregnated lignocellulosic material on pore development during phosphoric acid activation, Carbon 48 (2010) 3293–3311, https://doi.org/10.1016/j.carbon.2010.04.042.

[28] M. Şirazi, S. Aslan, Comprehensive characterization of high surface area activated carbon prepared from olive pomace by KOH activation, Chem. Eng. Commun. 208 (2021) 1479–1493, https://doi.org/10.1080/00986445.2020.1864628.

[29] R. Wang, P. Wang, X. Tan, J. Lang, C. Peng, Q. Xue, Promising porous carbon derived from celtuce leaves with outstanding supercapacitance and CO_2 capture performance, ACS Appl. Mater. Interfaces 4 (2012) 5800–5806, https://doi.org/10.1021/am302077c.

[30] M. Puig-Gamero, M. Fernandez-Lopez, P. Sánchez, J.L. Valverde, L. Sanchez-Silva, Pyrolysis process using a bench scale high pressure thermobalance, Fuel Process. Technol. 167 (2017) 345–354, https://doi.org/10.1016/J.FUPROC.2017.07.020.

[31] A. Villardon, A. Alcazar-Ruiz, F. Dorado, L. Sanchez-Silva, Enhancing carbon dioxide uptake in biochar derived from husk biomasses: optimizing biomass particle size and steam activation conditions, J. Environ. Chem. Eng. 12 (2024) 113352, https://doi.org/10.1016/j.jece.2024.113352.

[32] V. Chiodo, G. Zafarana, S. Maisano, S. Freni, F. Urbani, Pyrolysis of different biomass: direct comparison among Posidonia Oceanica, Lacustrine Alga and White-Pine, Fuel 164 (2016) 220–227, https://doi.org/10.1016/j.fuel.2015.09.093.

[33] N. Czerwinska, C. Giosuè, I. Matos, S. Sabbatini, M.L. Ruello, M. Bernardo, Development of activated carbons derived from wastes: coffee grounds and olive stones as potential porous materials for air depollution, Sci. Total Environ. 914 (2024) 169898, https://doi.org/10.1016/j.scitotenv.2024.169898.

[34] X. Xiao, B. Chen, Z. Chen, L. Zhu, J.L. Schnoor, Insight into multiple and multilevel structures of biochars and their potential environmental applications: a critical review, Environ. Sci. Technol. 52 (2018) 5027–5047, https://doi.org/10.1021/acs.est.7b06487.

[35] C. Wen, T. Liu, D. Wang, Y. Wang, H. Chen, G. Luo, Z. Zhou, C. Li, M. Xu, Biochar as the effective adsorbent to combustion gaseous pollutants: preparation, activation, functionalization and the adsorption mechanisms, Prog. Energy Combust. Sci. 99 (2023) 101098, https://doi.org/10.1016/j.pecs.2023.101098.

[36] S. Taghavi, E. Ghedini, M. Peurla, G. Cruciani, F. Menegazzo, D.Y. Murzin, M. Signoretto, Activated biochars as sustainable and effective supports for hydrogenations, Carbon Trends 13 (2023) 100316, https://doi.org/10.1016/j.cartre.2023.100316.

[37] K.A. Spokas, Review of the stability of biochar in soils: predictability of O:C molar ratios, Carbon. Manag. 1 (2010) 289–303, https://doi.org/10.4155/cmt.10.32.

[38] S. Schimmelpfenning, B. Glaser, One step forward characterization: some important material properties to distinguish biochars, J. Environ. Qual. 41 (2012) 1001–1013, https://doi.org/10.2134/jeq2011.0146.

[39] Z.A. Mayer, A. Apfelbacher, A. Hornung, A comparative study on the pyrolysis of metal- and ash-enriched wood and the combustion properties of the gained char, J. Anal. Appl. Pyrolysis 96 (2012) 196–202, https://doi.org/10.1016/J.JAAP.2012.04.007.
[40] S. Wang, G. Dai, H. Yang, Z., Luo Lignocellulosic biomass pyrolysis mechanism: a state-of-the-art review, Prog. Energy Combust. Sci. 62 (2017) 33–86, https://doi.org/10.1016/J.PECS.2017.05.004.
[41] A. Alcazar-Ruiz, F. Dorado, L. Sanchez-Silva, Bio-phenolic compounds production through fast pyrolysis: demineralizing olive pomace pretreatments, Food Bioprod. Process. 137 (2022) 200, https://doi.org/10.2139/ssrn.4117030.
[42] I.N. Raupp, A.V. Filho, A.L. Arim, A.R. Costa Muniz, G.S. Rosa, Development and characterization of activated carbon from olive pomace: experimental design, kinetic and equilibrium studies in nimesulide adsorption, Materials 14 (2021) 6820, https://doi.org/10.3390/ma14226820.
[43] J.M. Monteaguado, A. Duràn, M. Mänttäri, S. López, Insights into the adsorption of CO_2 generated from synthetic urban wastewater treatment on olive pomace biochar, J. Environ. Manag. 339 (2023) 117951, https://doi.org/10.1016/j.jenvman.2023.117951.
[44] S.A. Sadeek, E.A. Mohammed, M. Shaban, M.T.H. Abou Kana, N.A. Negm, Synthesis, characterization and catalytic performances of activated carbon-doped transition metals during biofuel production from waste cooking oils, J. Mol. Liq. 306 (2020) 112749, https://doi.org/10.1016/j.molliq.2020.112749.
[45] N. Kaya, M. Atagur, O. Akyuz, Y. Seki, M. Sarikanat, M. Sutcu, M.O. Seydibeyoglu, K. Sever, Fabrication and characterization of olive pomace filled PP composites, Compos. Part B 150 (2018) 277–283, https://doi.org/10.1016/j.compositesb.2017.08.017.
[46] S.O. Abdelhaidi, C.G. Dosoretz, G. Rytwo, Y. Gerchman, H. Azaizeh, Production of biochar from olive mill solid waste for heavy metal removal, Bioresour. Technol. 244 (2017) 759–767, https://doi.org/10.1016/j.biortech.2017.08.013.
[47] Y. Kavdır, R. İlay, O.B. Güven, A. Sungur, Characterization of olive pomace biochar produced at different temperatures and their temporal effects on soil aggregation and carbon content, Biomass Convers. Biorefinery (2023), https://doi.org/10.1007/s13399-023-03900-y.
[48] M. Thommes, K. Kaneko, A.V. Neimark, J.P. Olivier, F. Rodriguez-Reinoso, J. Rouquerol, K.S.W. Sing, Physisorption of gases, with special reference to the evaluation of surface area and pore size distribution (IUPAC Technical Report), Pure Appl. Chem. 87 (2015) 1051–1069, https://doi.org/10.1515/pac-2014-1117.
[49] D.D. Sewu, H. Jung, S.S. Kim, D.S. Lee, S.H. Woo, Decolorization of cationic and anionic dye-laden wastewater by steam-activated biochar produced at an industrial-scale from spent mushroom substrate, Bioresour. Technol. 277 (2019) 77–86, https://doi.org/10.1016/j.biortech.2019.01.034.
[50] K. Li, D. Zhang, X. Niu, H. Guo, Y. Yu, Z. Tang, Z. Lin, M. Fu, Insights into CO2 adsorption on KOH-activated biochars derived from the mixed sewage sludge and pine sawdust, Sci. Total Environ. 826 (2022) 154133, https://doi.org/10.1016/j.scitotenv.2022.154133.
[51] C. Quan, Y. Zhou, J. Wang, C. Wu, N. Gao, Biomass-based carbon materials for CO_2 capture: a review, J. CO2 Util. 68 (2023) 102373, https://doi.org/10.1016/j.jcou.2022.102373.
[52] C. Kim, S.N. Talapaneni, L. Dai, Porus carbon materials for CO2 capture, storage and electrochemical conversion, Mater. Rep. Energy 3 (2023) 100199, https://doi.org/10.1016/j.matre.2023.100199.
[53] A.D. Igalavithana, S.W. Choi, J. Shang, A. Hanif, P.D. Dissanayake, D.C. Tsang, J. H. Kwon, K.B. Lee, Y.S. Ok, Carbon dioxide capture in biochar produced from pine sawdust and paper mill sludge: effect of porous structure and surface chemistry, Sci. Total Environ. 739 (2020) 139845, https://doi.org/10.1016/j.scitotenv.2020.139845.
[54] L. Cao, X. Zhang, Y. Xu, W. Xiang, R. Wang, F. Ding, P. Hong, B. Gao, Straw and wood based biochar for CO_2 capture: adsorption performance and governing mechanisms, Sep. Purif. Technol. 287 (2022) 120592, https://doi.org/10.1016/j.seppur.2022.120592.
[55] F. Gao, Y. Li, Z. Bian, J. Hu, H. Liu, Dynamic hydrophobic hindrance effect of zeolite@ zeolitic imidazolate framework composites for CO_2 capture in the presence of water, J. Mater. Chem. A 3 (2015) 8091–8097, https://doi.org/10.1039/c4ta06645f.
[56] N. Querejeta, M.V. Gil, F. Rubiera, C. Pevida, Prospects of low-temperature solid sorbents in industrial CO_2 capture: a focus on biomass residues as precursor material, Greenhouse, Gas. Sci. Technol. 13 (2023) 245–284, https://doi.org/10.1002/ghg.2210.